


Interactions between cold cyclonic eddies and a western boundary current modulate marine heatwaves

Junde Li ^{1,2,3}✉, Moninya Roughan ¹ & Michael Hemming¹

Marine heatwaves are known to cause severe ecosystem damage and therefore have received attention in recent years. However, the focus has tended to be on global (surface) studies, but not coastal waters. Cyclonic eddies are important and underappreciated components in the eddy-dominated western boundary current system, but their impacts on the path of the western boundary currents have largely been unexplored. Here we show that cold cyclonic eddies can modulate the most intense coastal marine heatwaves on record inshore of the East Australian Current. We show that the marine heatwave was driven and modulated by the lateral movement of the western boundary current jet and cyclonic eddies. This study reveals that the interplay of cyclonic eddies and a western boundary current can drive coastal ocean warming, paving the way for future investigations into eddy interactions and the evolution of coastal marine heatwaves in other western boundary current regions.

¹School of Biological Earth and Environmental Sciences, University of New South Wales, Sydney, NSW, Australia. ²Key Laboratory of Marine Hazards Forecasting, Ministry of Natural Resources, Hohai University, Nanjing, China. ³College of Oceanography, Hohai University, Nanjing, China. ✉email: junde.li@unsw.edu.au

Marine heatwaves (MHWs) are prolonged discrete extreme oceanic warm water events¹. The probability of the occurrence of severe MHWs has increased due to anthropogenic climate change² and it is projected that MHWs will become more frequent and extreme under continued global warming³. Severe MHWs have already been shown to push some marine organisms and ecosystems beyond their upper thermal limits and heat stress tolerance. This can potentially cause irreversible changes³, leading to devastating impacts on marine ecosystems^{4,5} and commercial fisheries^{6,7} with vast socio-economic consequences⁸.

Many populous cities are located by the coast, and coastal oceans support productive marine ecosystems⁹, therefore, coastal MHWs can have the greatest effects on biodiversity, productivity, coastal climate, and urban thermal environments¹⁰. In addition, coastal MHWs have dramatic influences on diverse coastal communities, showing an increase in occurrence probability, duration, and intensity over the past decades^{10,11}. Compared to offshore MHWs, our understanding of coastal MHWs is limited¹², yet due to the disproportionately high productivity in coastal regions, there is a pressing need to investigate the evolution and physical processes driving coastal MHWs.

MHWs have been widely reported in many parts of the global ocean over the past decade⁸. The western boundary current (WBC) extension regions have large horizontal sea surface temperature (SST) gradients and are hot spots of high MHW frequency and intensity^{13,14}. In the Southern Hemisphere, a poleward penetration of WBCs is driving ocean warming^{15,16} and increased eddying in their extensions^{16,17}. As a WBC of the South Pacific Ocean, the East Australian Current (EAC) flows poleward along southeastern Australia, transporting tropical warm water to higher latitudes. Previous studies have investigated the characteristics and drivers of offshore MHWs in the EAC^{18–20}. For example, surface air-sea heat flux drives shallower MHWs in the EAC upstream jet, which are most prevalent in summer, but the deepest and longest MHWs in the EAC southern extension are predominantly driven by horizontal advection within eddies¹⁹. An intensified EAC southern extension caused the 2015/16 Tasman Sea MHW, which lasted 251 days with a maximum SST anomaly (SSTA) of 2.9 °C, resulting in an outbreak of oyster disease, mortality of blacklip abalone and out-of-range species observations²¹.

Inshore of the EAC jet, coastal shelf waters are warming nonuniformly along the EAC path, with a faster warming rate poleward of 32 °S due to an increase in lateral heat advection²². In addition, subsurface coastal MHWs on the southeastern Australian continental shelf (34 °S) can be driven by local downwelling favorable winds²³. In the 2021/22 austral summer, coastal waters off Sydney Australia (34 °S) experienced their hottest temperatures on record (Fig. 1). This was despite a prolonged La Niña responsible for cooler atmospheric temperatures, large-scale rainfall and widespread flooding²⁴. Hence, this coastal MHW was unexpected and the drivers were unknown.

The EAC typically separates from the coast between 31 °S–32.5 °S in a region of complex eddy interactions²⁵. Large anticyclonic eddies shed from the main EAC jet due to barotropic instabilities during separation^{16,26–28}. Approximately 88% of mesoscale eddies in the EAC system propagate westward²⁹. Cyclonic eddies propagating into the typical EAC separation region from the east have the potential to interact with the EAC jet^{30–32}, impacting chlorophyll concentrations³³, but these interactions have largely been unexplored. In addition, smaller cyclonic eddies often form as frontal eddies on the inside edge of the EAC jet^{34–36}. Downstream of the separation point, counter-rotating eddy dipoles can form, driving cross-shelf transport^{37,38} and pushing warm water onto the shelf²². However, the role of

these cyclonic eddies in modulating the lateral movement of the EAC or WBCs more broadly remains to be explored.

In this study, we use satellite observations combined with atmosphere and ocean reanalysis products to diagnose the physical drivers of the strong coastal MHWs that occurred off Sydney in the austral summer of 2021/22. First, we characterise the coastal MHWs from satellite and sub-surface in situ observations. Then, we investigate the contributions of atmospheric forcing and oceanic advection to temperature changes during the MHW events using a heat budget approach. Finally, exploring 30 historical MHW events, we demonstrate the role of cyclonic eddies in modulating the position of the EAC jet and driving MHWs.

Results

Two coastal MHWs in the austral summer of 2021/22. In the 2021/22 austral summer (December–February), the SST warming in the western Tasman Sea was nonuniform. In December 2021, most regions north of 36 °S were warming (Fig. 1a) and a persistent warm anomaly was evident confined to the EAC path. However, east of the EAC jet (delineated by the solid black line) and north of 33 °S, the waters are anomalously cool during January–February 2022 (Fig. 1b, c). During these three months, the largest warming occurred downstream of the typical EAC separation point within a latitude range of 32 °S–36 °S. Inshore of the EAC jet, coastal waters off Sydney were anomalously warm (green box in Fig. 1a–c, hereafter referred to as the Sydney Box), which is the focus of this study.

We averaged the monthly SSTA for December, January, and February in the Sydney Box over the past three decades (1993–2022) (Supplementary Fig. S1). The austral summer of 2021/22 shows the largest SSTA since 1993, with monthly mean SSTA reaching up to 1.59 °C in December 2021, 0.83 °C in January 2022, and 1.41 °C in February 2022, respectively. This is consistent with news reports of coastal waters off Sydney during the austral summer of 2021/22²⁴, being the hottest summer on record since 1993. The evolution of daily SST within the Sydney Box shows that two MHWs occurred (Fig. 1d). The first severe MHW started on 13 December 2021 and lasted 27 days, reaching a maximum intensity of 2.02 °C above climatology. The second strong MHW had a similar duration of 28 days (29 January–25 February 2022), but with a maximum intensity of 1.20 °C. These two events were punctuated by a cooler period in mid January 2022.

These coastal MHWs not only impacted the surface temperature but also penetrated into the subsurface layers (Fig. 2). Using in situ mooring observations at two sites (SYD100 and PH100) close to the 100 m isobath off Sydney (Fig. 2a), we observe two MHWs in December 2021 and February 2022. The temperature anomalies extend through the water column between 18 m depth and the bottom and at some depths, the anomalies are greater than at the surface. At the SYD100 location, the temperature anomalies relative to the mean at 32 m have a maximum intensity of 5 °C on 28 December, 2021 and 4.9 °C on 12 February, 2022 (Fig. 2c). Although the temperature anomalies in February at SYD100 were higher than the 90th percentile below the surface, they fluctuated just enough for the event to not be classified by the standard MHW definition of 5 days duration.

The PH100 mooring observed similar subsurface temperature anomalies relative to the mean (90th percentile) at 34 m, with a maximum intensity of 5.8 (4.2) °C on 27 December 2021 and 4.5 (2) °C on 12 February 2022 (Fig. 2f). In contrast to surface temperature from satellite observations (Fig. 2b, e), the subsurface experienced cooling in January 2022 at the two Sydney mooring locations (Fig. 2c, f), shown as several moderate marine cold spells/cold spikes (Fig. 2d, g). The subsurface intensified warming

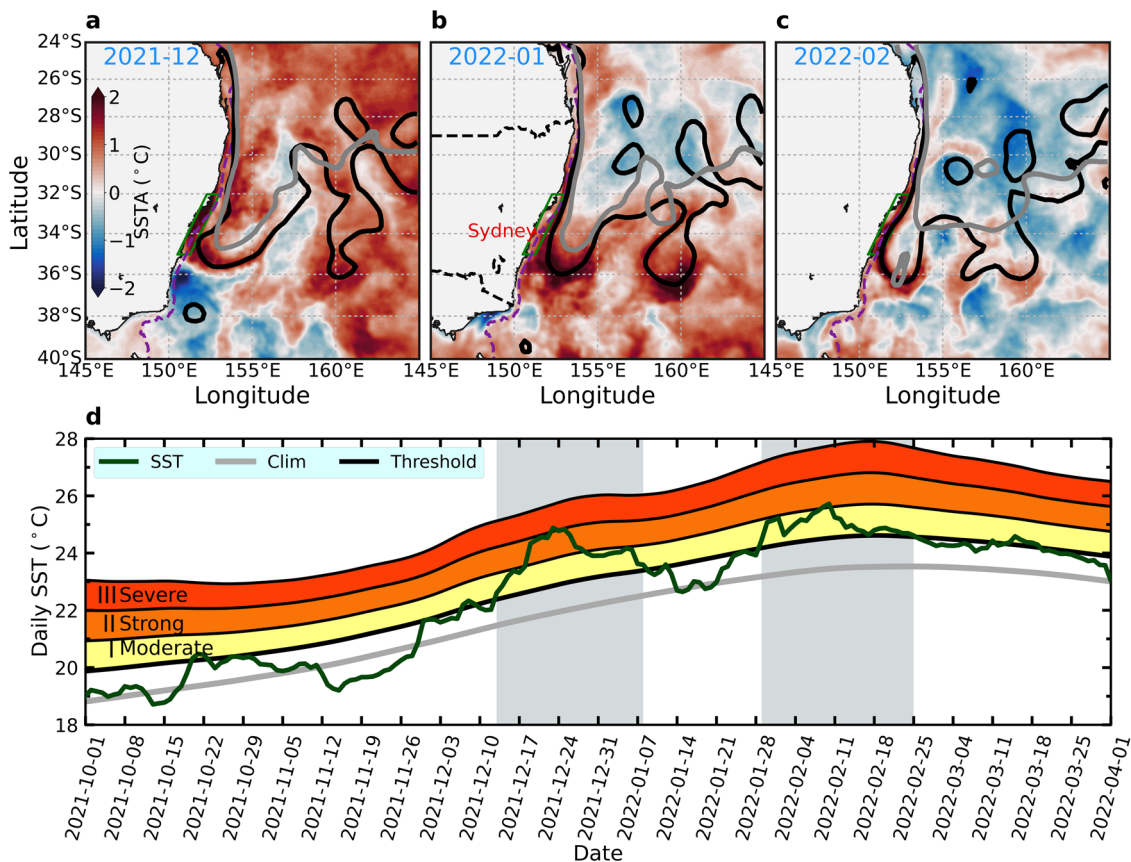


Fig. 1 Observed SSTA from OSTIA observations in the austral summer of 2021/22. **a** Spatial distributions of monthly mean SSTA from OSTIA observations in December 2021. The green box indicates the Sydney Box ($\sim 32.6^{\circ}\text{S}$ – 35.1°S , $\sim 150.4^{\circ}\text{E}$ – 152.6°E). The dashed purple, solid black and gray lines indicate the 200 m isobath, the 0.95 m contour of observed monthly mean sea surface height (SSH) and the monthly climatological mean SSH (1993–2022), respectively. **b**, **c** Same as **a** but for January 2022 and February 2022, respectively. **d** Time series of daily SST observations (green line), SST climatology (gray line) and the 90th percentile threshold (black line) averaged within the Sydney Box from 1 October 2021 to 1 April 2022. The MHWs are shaded in gray color. MHW severity categories I ('Moderate'), II ('Strong') and III ('Severe') are shaded in yellow, orange and red, respectively.

and cooling suggests that ocean dynamics played an important role in temperature variability at that time. In the following sections, we discuss the dynamics responsible for driving and modulating these two coastal MHWs.

Physical drivers of coastal MHWs. To investigate the mechanisms driving and modulating the two coastal MHWs in the Sydney Box, we first show the spatial distributions of the kinetic energy (Fig. 3a–c). During our study period, the EAC penetrated further south to around 36°S (black lines in Figs. 1a–c and 3a–c). Compared to normal years (gray lines in Figs. 1a–c and 3a–c), the EAC jet meandered eastward at $\sim 32^{\circ}\text{S}$, propagating onshore and re-attaching to the coast at $\sim 34^{\circ}\text{S}$ during December 2021. In January and February, the EAC jet flowed poleward to around 36°S with its major axis offshore in January and onshore in February (Fig. 3b, c). An anomalous poleward penetration of the EAC transported more warm water to the downstream regions. As a result, we see anomalous warming along the EAC path between 32°S and 36°S (Fig. 1a–c).

Next, we examine the air-sea heat flux anomalies (Fig. 3d–f). Although the ocean gained heat from the atmosphere in some regions of the western Tasman Sea, particularly in December, we found negative air-sea heat flux anomalies along the EAC path (Fig. 3d), suggesting that the ocean lost heat to the atmosphere and the warming was driven by the ocean circulation instead of the air-sea heat flux. In January and February 2022, more heat was released from the ocean to the atmosphere along the EAC

path (Fig. 3e, f), particularly in February 2022, as is expected in a western boundary current. In the Sydney Box, the negative air-sea heat flux anomalies imply that atmospheric forcing made no contribution to the development of these two coastal MHWs. Therefore, we can deduce that ocean circulation plays a dominant role in driving these coastal MHWs.

To further elucidate the physical mechanisms responsible for the temperature changes within the Sydney Box, we conduct a mixed layer heat budget analysis (Fig. 4). The evolution of all terms contributing to the heat budget within the mixed layer are shown in Fig. 4a, from 1 December 2021 to 28 February 2022. The horizontal advection terms dominate the temperature changes ($TTEND$, orange), and the processes associated with horizontal diffusion, vertical diffusion, and unresolved subgrid-scale uncertainty also make some contributions ($Residual$, green). The zonal advection ($UADV$, red) makes the greatest contribution to ocean warming, whereas the meridional advection ($VADV$, purple) plays the opposite role and decreases temperature. The balance between warming induced by zonal advection and cooling resulting from meridional advection primarily controls the temperature changes in the Sydney Box. The zonal advection continuously increases the temperature during this period (01/12/2021–28/02/2022), with a peak warming rate of 1.71°C per day on 21 February 2022. However, the vertical entrainment term ($ENTR$, gray) is negligible. In comparison, the net air-sea flux term (Q , blue) is much smaller and negative most of the time, which further verifies that the MHWs were not driven by anomalous air-sea heat flux.

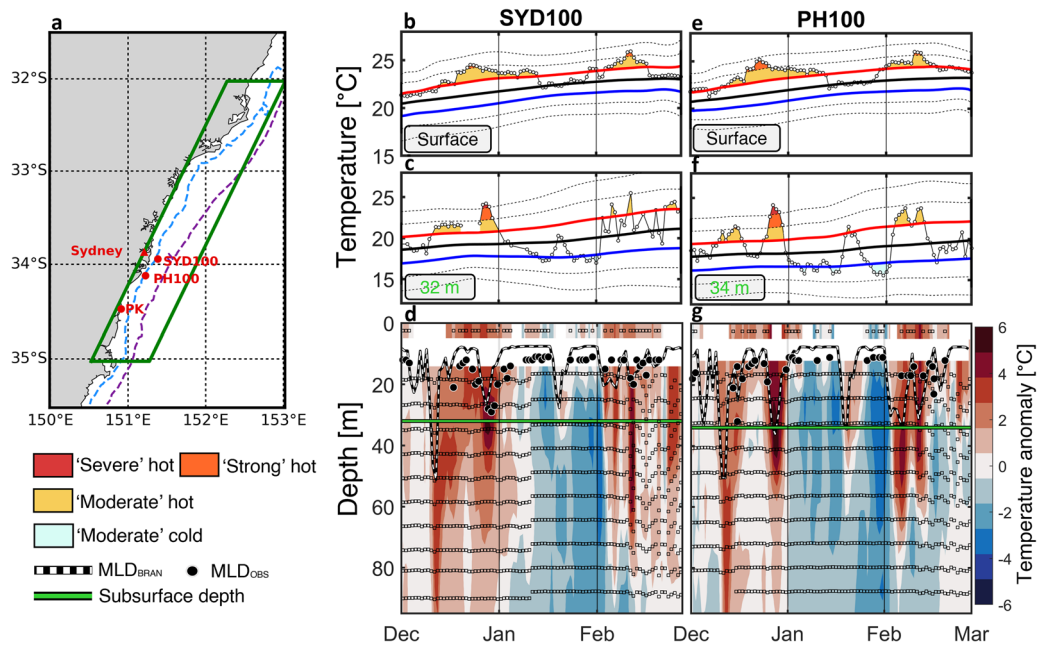


Fig. 2 Observed temperature anomalies in the austral summer of 2021/22 from 2 moorings along the 100 m isobath off the Sydney coast. Satellite temperature data is also included at the surface. **a** Map showing the locations of the moorings (SYD100 and PH100) at the 100 m isobath and the Port Kembla tide gauge station (PK). The dashed purple and blue lines indicate the 200 m and 100 m isobath, respectively. The green box indicates the Sydney Box. **b** The MHW surface temperatures from satellite observations (1993–2022) at SYD100. The 10th and 90th percentiles and mean, are shown as blue, red, and black lines, respectively. The MHW severity categories I (‘Moderate’ hot, yellow / blue depending on whether it’s a hot or cold event, respectively), II (‘Strong’, orange), and III (‘Severe’, red) are represented by dashed black lines and have accompanying text annotations. **c** Same as **b** but for a depth of 32 m from the moored data. **d** The subsurface temperature anomalies (relative to the daily mean climatology) from the full depth mooring are shown during the same time period at SYD100. The vertical linearly interpolated temperature anomalies are shown, with the depths of the daily-binned mooring observations overlaid as hollow black squares. The horizontal green line indicates the depths of the observed temperatures in **(c)**. The white-black line and the black dots indicate the mixed layer depth from the BRAN2020 reanalysis and in situ moored observations, respectively. **e–g** Same as **b–d** but for the PH100 mooring, where the selected depth in **(f)** is 34 m at PH100.

Here we demonstrate the contributions of the monthly mean horizontal advection and air-sea heat flux to temperature changes within the Sydney Box. Both the meridional advection and the air-sea heat flux are negative in all three months (Fig. 4b). The cooling rate of meridional advection increases from 0.12 °C per day in December 2021 to 0.50 °C per day in February 2022. However, zonal advection has a warming rate of 0.24 °C per day in December 2021 and 0.92 °C per day in February 2022, which compensates for the ocean cooling in the other terms and contributes strongly to the observed ocean warming.

Spatial distributions of temperature changes, horizontal advection and air-sea heat flux further emphasise the important role of horizontal advection in modulating temperature changes in the western Tasman Sea (Fig. 4c–n). In December 2021, we found strong positive zonal advection (Fig. 4d) but weak negative meridional advection (Fig. 4e) inshore of the EAC jet between 30°S and 35°S, particularly in the Sydney Box. Both positive zonal advection and negative meridional advection inshore of the EAC jet intensified in January 2022 (Fig. 4h, i), but the maximum horizontal advection tended to be offshore due to the eastward movement of the EAC major axis (Fig. 3b). In February 2022, the EAC jet encroached upon the Sydney coast (Fig. 3c), resulting in strong positive zonal advection (Fig. 4l) and negative meridional advection (Fig. 4m) between 33°S and 35°S. Therefore, the lateral movement (eastward and westward) of the EAC major axis plays a key role in the heat transport from the warm EAC and the regions of high ocean heat content to coastal regions.

Lateral movement of the EAC. The sea level anomalies (SLA) in Fig. 3g–i show large cyclonic eddies in the EAC separation region, suggesting that cyclonic eddies may play a role in modulating the position of the EAC jet and its associated anticyclonic eddies in this region, which we further explore here. In December 2021, a large anticyclonic eddy (warm core, anticlockwise rotating, AE) shed from the EAC jet at around 34°S where it separated from the coast and turned eastward (Fig. 3g). In the meantime, the EAC jet was surrounded by cyclonic eddies (cold core, clockwise rotating, CE). As shown in Fig. 3g, a small cyclonic frontal eddy formed inshore of the EAC jet (CE1), and two large cyclonic eddies are evident. One CE originating from the EAC eastern extension was located east of the EAC return flow (CE2) (the northern branch of the EAC after it separates from the coast). The other CE was located south of the EAC jet (CE3) forming while the EAC separated from the coast.

During January, negative SLA dominated the coastal shelf inshore of the EAC jet between 32°S and 36°S and south of the EAC separation point, suggesting that the frontal eddy merged into CE3 (Fig. 3h). This frontal eddy disappeared when the EAC jet moved onshore toward the Sydney coast in February 2022 (Fig. 3i). However, both CE2 and CE3 were still located east of the EAC return flow and south of the EAC separation point, respectively. SLA data shows that CE2 continued to move westward from December 2021 to February 2022 (Fig. 3g–i) and became stronger and more coherent by February (Fig. 3i).

Cyclonic eddies are characterized by cold waters within their cores. Frontal eddies that form inshore of WBCs can entrain colder shelf waters and propagate poleward^{35,36}, further

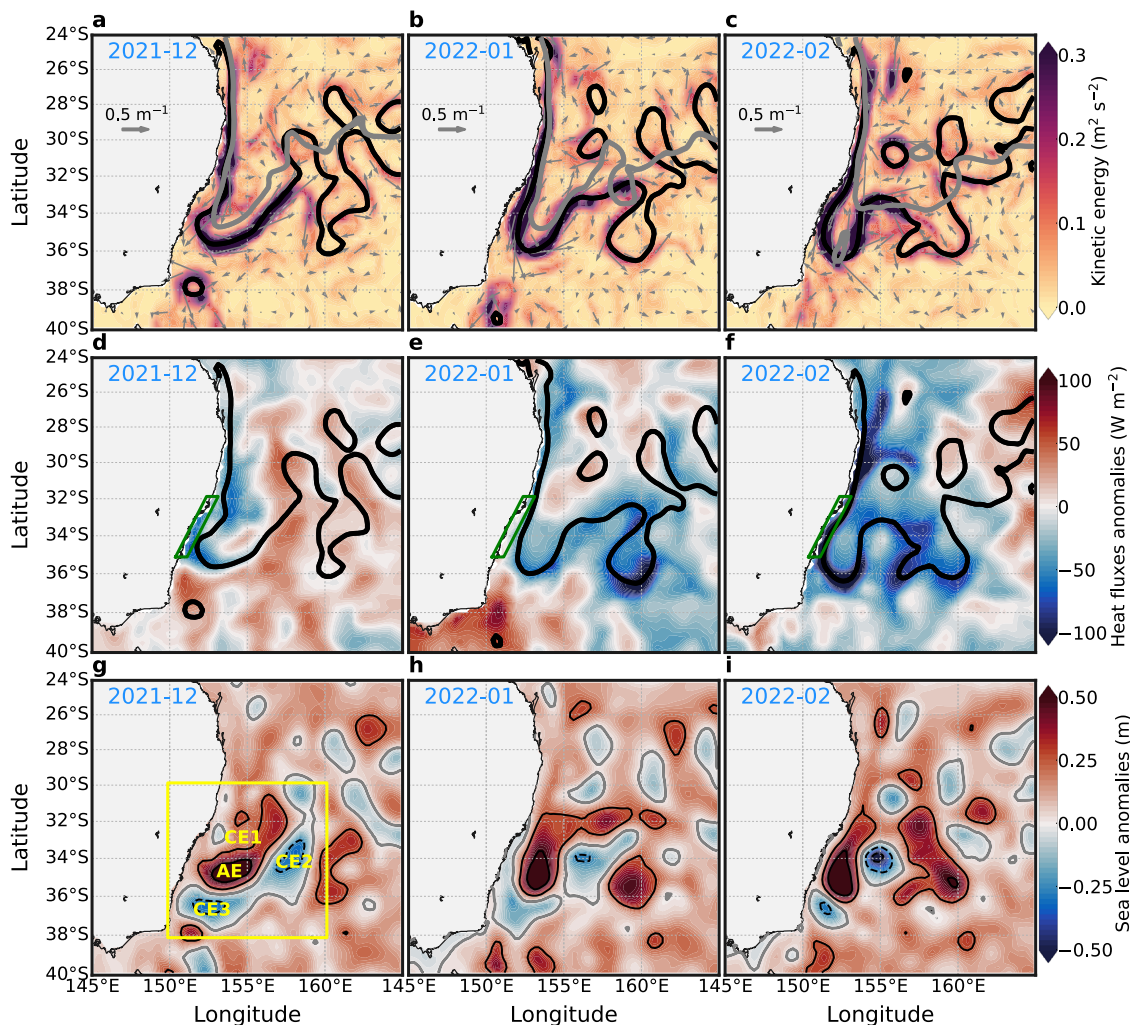


Fig. 3 Spatial distributions of kinetic energy, heat flux anomalies and SLA in the austral summer of 2021/22. **a** Monthly mean surface kinetic energy from AVISO observations in December 2021. The thick black and gray lines indicate the 0.95 m contour of observed monthly mean SSH in each month and the monthly climatological mean SSH (1993–2022), respectively. The gray vectors indicate the surface geostrophic velocities. **b, c** Same as **a** but for January 2022 and February 2022, respectively. **d–f** Same as **a–c** but for the air-sea heat flux anomalies at the ocean surface from ERA5. Positive anomalies represent heat gain by the ocean and negative anomalies represent heat loss from the ocean. The green boxes in (**d–f**) indicate the Sydney Box. **g–i** Same as **a–c** but for the SLA from AVISO observations. The solid black line, gray line and dashed black line in (**g–i**) indicate the positive, zero and negative SLA, respectively. The yellow box in (**g**) denotes the domain in Figs. 4, 5 and the eddies discussed in the text are labelled as cyclonic eddy (CE) 1–3 and anticyclonic eddy (AE).

impacting the temperature changes along the path³⁴. The larger cyclonic eddies CE2 and CE3 (Fig. 3g) are much stronger than the frontal eddy, and their interactions with the EAC could impact the movement of the jet and heat transport in the region.

To illustrate how these cyclonic eddies may impact the evolution of MHWs in the Sydney Box, we examine the spatial distributions of weekly SLA between 28°S and 38°S (Fig. 5a–l). Compared to the monthly mean SLA (Fig. 3g–i), weekly SLA can better resolve the evolution and propagation of cyclonic eddies, which allows us to investigate the interactions between cyclonic eddies and the EAC jet. A strong frontal eddy formed inshore of the EAC jet between 32°S and 33.5°S (Fig. 5a) in early December 2021. This frontal eddy propagated southwestward during the period of 01/12/2021–05/01/2022, but did not encroach into the coastal shelf (Fig. 5a–e), so coastal temperatures remained elevated in the Sydney Box and governed by the EAC. Here the EAC jet attached anomalously close to the coast, pushing warm water into the coastal region. SLA was positive in the Sydney Box

(Figs. 5a–e and 6a), corresponding to positive SSTA above the 90th percentile averaged over this region (Fig. 1d).

When this frontal eddy propagated further southwestward from 5 January 2022 to 26 January 2022 (Fig. 5f–i), it merged into the large cyclonic eddy CE3 (located immediately south of the EAC separation point), and may push the southern tip of the EAC jet offshore. As a result, this cyclonic frontal eddy propagated negative SLA into the Sydney Box, associated with an offshore movement of the EAC jet (black lines in Fig. 5). This resulted in the offshore movement of heat and the decay of the coastal MHW within the Sydney Box (Fig. 1d) while a MHW persisted offshore (Fig. 1b).

East of the EAC return flow (Fig. 5a, 158°E), we can see a large negative SLA (identified as CE2 by closed SLA contours in Fig. 3g). This large negative SLA propagated westward (Figs. 5 and 6a) and interacted with the large anticyclonic eddy (AE) that shed from the EAC jet, resulting in the westward movement of the anticyclonic eddy and the EAC jet, particularly after 5 January 2022 (Figs. 5f–l and 6a). When the EAC jet again moved

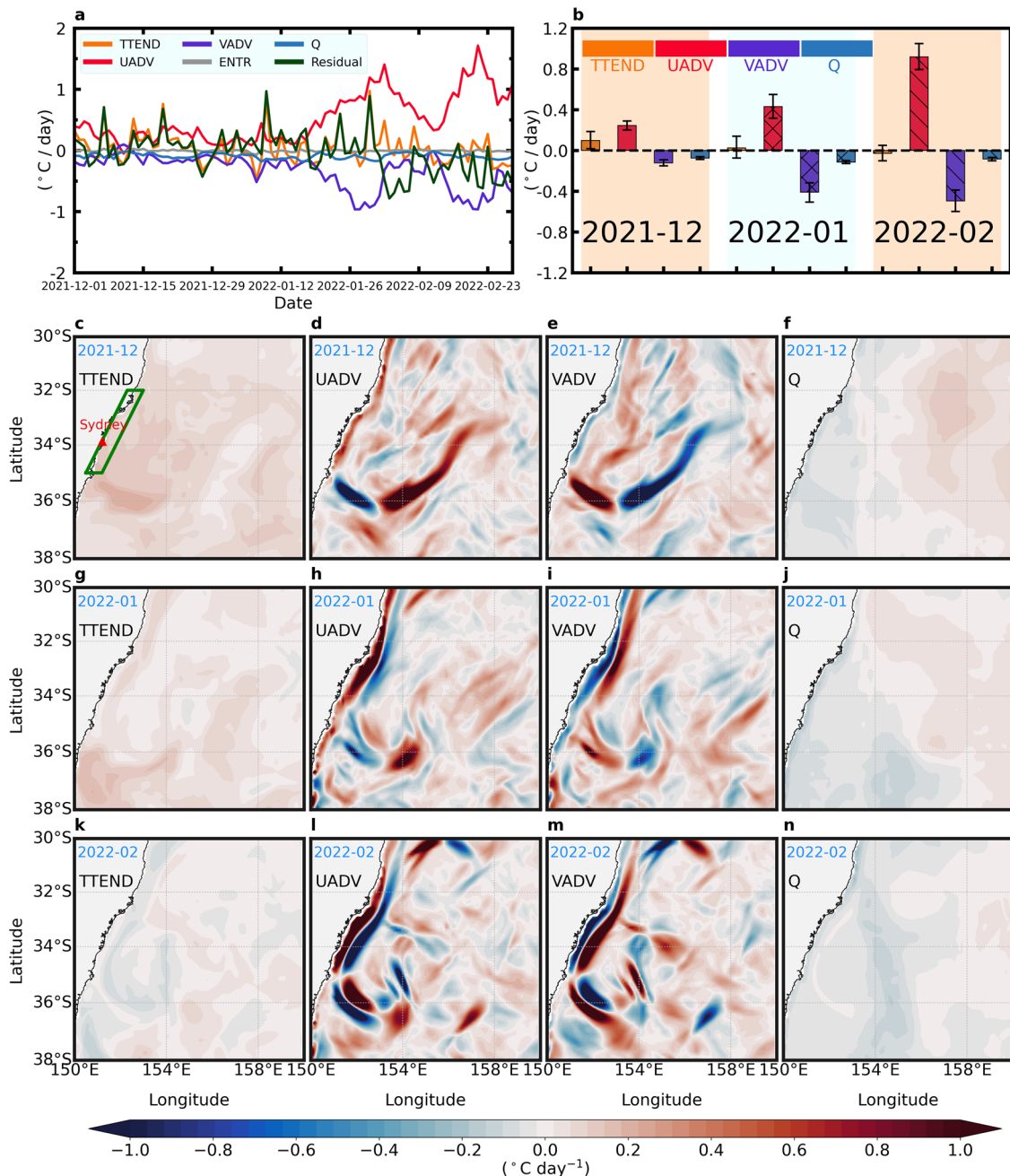


Fig. 4 Mixed layer heat budget in the austral summer of 2021/22. **a** Time series of the mixed layer heat budget terms averaged within the Sydney Box during the period of 01/12/2021–28/02/2022 from BRAN2020. The orange, red, purple, gray, blue and green lines indicate the temperature tendency, zonal advection, meridional advection, vertical entrainment, net air-sea heat flux and *Residual* term, respectively. **b** Monthly temperature tendency (orange bar), zonal advection (red bar), meridional advection (purple bar) and net air-sea heat flux (blue bar) averaged within the Sydney Box for December 2021, January 2022, and February 2022. Error bars represent 95% confidence intervals. **c** Spatial distributions of monthly mean temperature tendency in December 2021. The green box indicates the Sydney Box. **d–f** Same as **c** but for the zonal advection, meridional advection and net air-sea heat flux, respectively. **g–j** Same as **c–f** but for January 2022. **k–n** Same as **c–f** but for February 2022.

westward and attached to the coast starting in late January, it transported warm waters to the shelf. Thus, we can see strong positive zonal advection (Fig. 4a, l), which drives the second MHW within the Sydney Box from late January to middle February 2022.

The evolution of SLA averaged over the Sydney Box further shows the impact of eddies on coastal regions (Fig. 6b). Positive SLA was observed in December 2021 and February 2022 (Fig. 6b), corresponding to the periods of MHWs (Fig. 1d). The periods of negative SLA are consistent with those of the southwestward

propagation of the frontal eddy (Figs. 5f–i and 6a) and the subsurface marine cold spells (Fig. 2d, g). To further demonstrate the consistent variations of SLA and SSTA near the coast, we show the SLA measured in situ at the Port Kembla (PK) tide gauge (location shown in Fig. 2a), compared with data from the BRAN2020 reanalysis and AVISO satellite observations. The evolution of SLA in all three datasets is overall in good agreement, showing positive anomalies during the December 2021 and February 2022 MHWs and negative anomalies during the January 2022 subsurface marine cold spell period. Small discrepancies

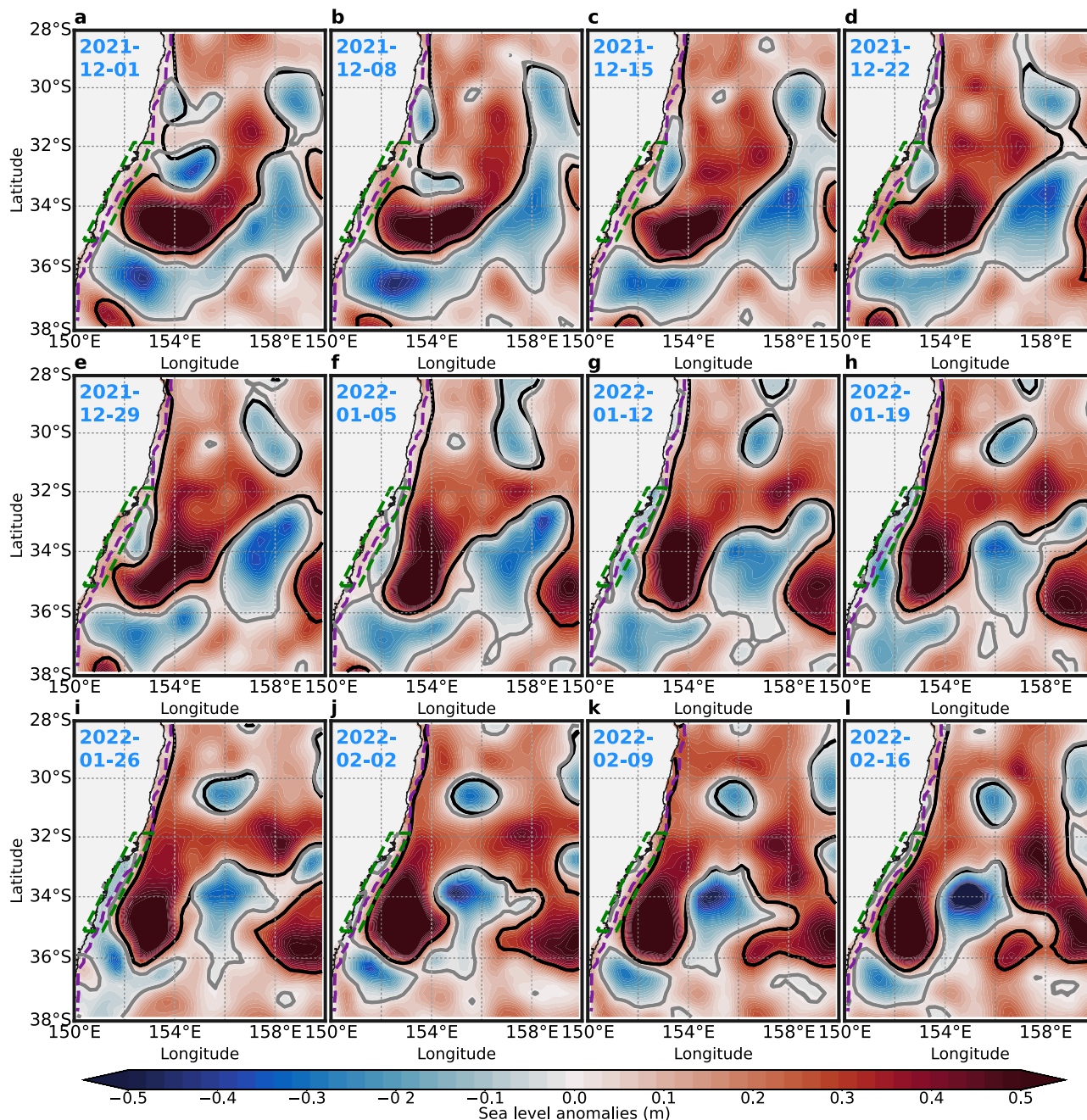


Fig. 5 Spatial distributions of AVISO daily SLA observations in the austral summer of 2021/22. **a** Spatial distributions of SLA on 1 December 2021. The thick black, gray and dashed purple lines indicate the 0.95 m

contour of observed daily SSH, zero SLA and the 200 m isobath, respectively. The green box indicates the Sydney Box. **b–l** Same as **a** but for the SLA from 8 December 2021 to 16 February 2022 every week.

between the datasets could be due to differences in resolution, model biases in BRAN2020, as well as challenges of the coarser AVISO satellite observations in shallow water. These data also indicate that the southwestward propagation of CE1 was responsible for the decay of the MHW in December 2021 and the subsurface cooling in January 2022.

By examining the SST evolution within the Sydney Box over the period of 1993–2022, we identified 30 MHWs in total. Among all these MHWs, the MHW that occurred in December 2021 is the strongest. A composite analysis from ten strong MHWs showed that these MHWs occurred when the EAC penetrated to the east of the Sydney Box and was accompanied by a large cyclonic eddy east of the EAC jet and a small cyclonic eddy south of the EAC separation point (Fig. 6c). In these cases when the

EAC jet penetrated poleward and brought more warm water to the regions east of the Sydney Box, the westward propagation of this large cyclonic eddy could cause the EAC jet to move westward and result in ocean warming in the Sydney Box.

Discussion

We examined the physical drivers of two coastal MHWs that occurred off Sydney (34°S) in the austral summer of 2021/22 using in situ and satellite observations, high-resolution ocean reanalysis and a mixed layer heat budget analysis. Our results showed that the maximum intensities of the two coastal MHWs within the Sydney Box reach up to 2.02 °C and 1.2 °C above climatology at the surface layer, respectively. We showed that the horizontal advection dominates the temperature changes in

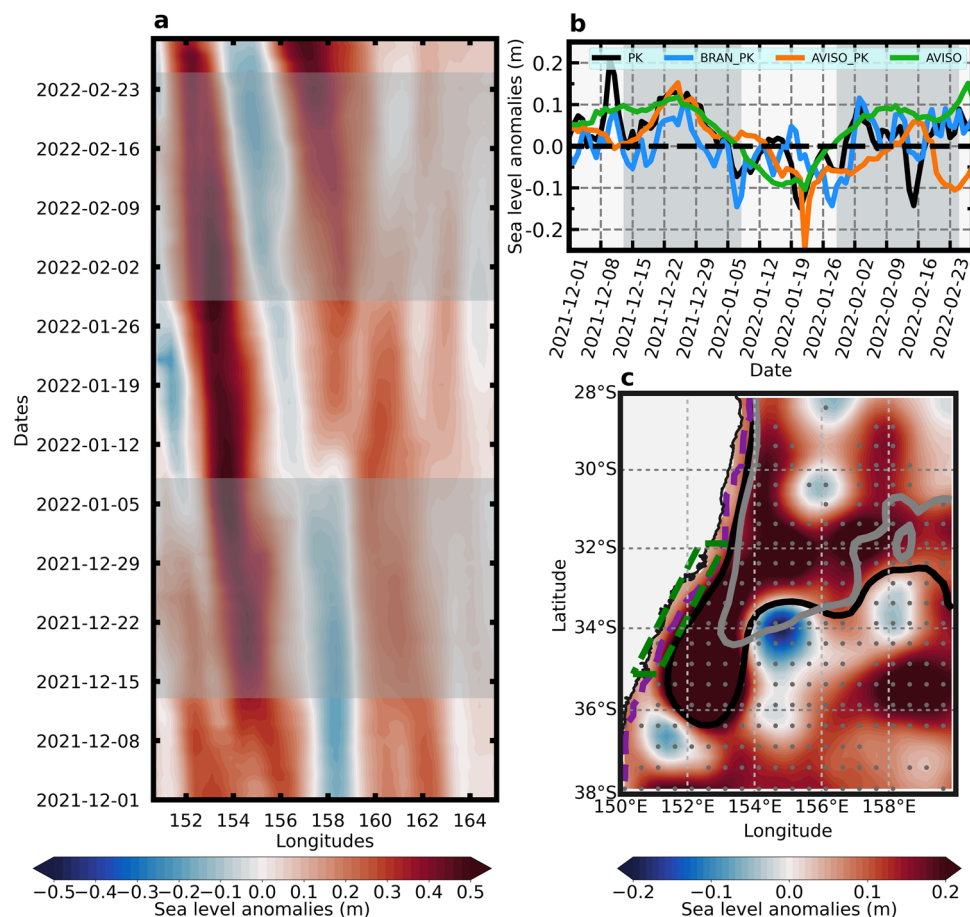


Fig. 6 Westward propagation and evolution of SLA around the Sydney Box in the austral summer of 2021/22. **a** Hovmöller plot of daily meridional mean SLA averaged within 32°S–35°S from the coast to 165°E during the austral summer of 2021/22. The periods of MHWs are shaded in gray color. **b** Time series of the SLA at the Port Kembla (PK) station from tide gauge observations (solid black line), BRAN2020 reanalysis (solid blue line) and AVISO satellite observations (solid orange line). The solid green line indicates the SLA averaged over the Sydney Box from AVISO observations. The dashed black line represents the zero sea level. **c** Spatial distributions of composite SLA for ten strong MHWs. The dashed purple, solid black and gray lines indicate the 200 m isobath, 0.95 m contour of composite SSH over the periods of ten MHWs and the climatological mean SSH (1993–2022), respectively. The green box indicates the Sydney Box. Gray stipples indicate the SLA anomalies that are statistically significant above the 95% confidence level.

the Sydney Box, and air-sea heat flux is negative and negligible. Further analysis of 30 historic MHWs suggested that cyclonic eddies can modulate the eastward and westward (lateral) movement of the EAC major axis. The westward propagation of mesoscale cyclonic eddies is associated with an onshore movement of the warm EAC jet, driving the MHWs in the coastal region. Whereas the frontal eddy drove negative sea level and temperature anomalies inshore of the EAC jet. These cyclonic eddies were responsible for the heat transport of the warm EAC both into and out of coastal regions. We showed that eddy interactions can modulate the evolution of coastal MHWs.

Eddy interactions are complex in WBC regions, this study reveals the role of cold cyclonic eddies in modulating the lateral movement of the EAC jet. Cyclonic eddies can move the warm jet both offshore (when frontal eddies form inshore of the jet) and onshore (when the cyclones propagate westward into the region). Small (Frontal)³⁶ and large cyclonic eddies are ubiquitous features of WBC regions³⁰, however, WBC cyclonic eddies are generally understudied compared to their warm counterparts and their dynamics and impacts deserve further investigation.

The mesoscale circulation patterns associated with the EAC jet^{37,39,40} and its eddy field^{41,42} dominate the circulation

offshore of the Sydney Box^{31,32,37,43}. Therefore, the interactions of the EAC jet and the mesoscale eddy field can play a role in the heat transport between offshore and onshore waters⁴⁴. Here we show that the propagation of the frontal eddy inshore of the EAC jet can modulate the position of the EAC jet (Figs. 5 and 6a), and in this case may cause the decay of a MHW. In addition, we showed that a westward propagating cyclonic eddy can modulate the lateral (onshore) movement of the WBC (Figs. 5 and 6a), resulting in coastal MHW events by pushing warm water onshore. This suggests that eddies could be one mechanism driving heat from offshore to onshore⁴⁴. Thus, it is important to understand the role of cyclones in modulating the positions of both the EAC jet and warm anticyclonic eddies.

Several studies have investigated the drivers of coastal MHWs. Overwhelmingly, they have found that local processes play a role in coastal MHWs due to the complex regional dynamics in coastal systems. While suppressed upwelling by a wind relaxation has been observed to drive MHWs in eastern boundary current systems, such as the California Current system⁴⁵ and the Chile-Peru Current⁴⁶, the drivers of MHWs in WBCs have not been explored thoroughly. In the Brazil Current (South Atlantic Ocean WBC), the Madden-Julian Oscillation might have played a leading role in setting the persistent extremely high air temperature and low wind speed, resulting in

the most intense MHWs occurring in the austral summer of 2017⁴⁷. In contrast, our results show that the air-sea heat flux did not drive the coastal MHWs, instead that the horizontal advection terms associated with the EAC (modulated by the cyclonic eddies) drove the temperature changes. Our study highlights that the impacts of cyclonic eddies and WBCs on coastal MHWs need further investigation. Our results have far-reaching implications for understanding the role of cyclonic eddies in WBCs as well as for investigating the physical drivers of coastal MHWs in other WBC regions.

Recent studies have identified an increase in eddy activity in the poleward extensions of the WBCs of the southern hemisphere^{16,17}. As the offshore region is experiencing an increase in SST and eddy activity¹⁶, eddies could be one mechanism driving heat from offshore to onshore⁴⁴. Thus understanding the role of eddies in driving the lateral movement of WBCs is important for understanding both marine extremes (heatwaves and coldspells) as well as the role of eddies in driving long term temperature trends in shelf waters.

Methods

Satellite observations. In this study, we use the latest Operational Sea Surface Temperature and Ice Analysis (OSTIA) to investigate MHWs⁴⁸. The OSTIA observations span 30 years from 1 January 1993 to 31 December 2022, with a horizontal resolution of $0.05^\circ \times 0.05^\circ$. The daily and monthly climatologies are calculated over the period of 1993–2022.

The daily satellite observations of SLA and geostrophic current velocities are obtained from Archiving, Validation and Interpretation of Satellite Oceanographic (AVISO)⁴⁹, which are distributed by the Copernicus Marine and Environment Monitoring Service (CMEMS). The AVISO observations have a horizontal resolution of $0.25^\circ \times 0.25^\circ$, which capture the eddy activity well in the EAC system^{16,28,50}.

In situ observations. We use in situ temperature observations measured by thermistors positioned at 8 m intervals between the near-surface and the sea bed at two moorings maintained by Australia's Integrated Marine Observing System (IMOS): the Port Hacking 100 m (PH100: 34.12°S, 151.22°E) and Sydney 100 m (SYD100: 33.94°S, 151.38°E) mooring sites⁵¹. We used the aggregated long time series products developed by the Australian Ocean Data Network (AODN). As the temporal sampling of the moored in situ sensors is 5 min, we created gridded products with daily resolution⁵².

To calculate in situ mooring temperature anomalies relative to the mean and the 90th percentiles, we created a daily climatology for each subsurface depth following⁵². A time-centered window of 11 days was used to calculate climatology statistics, followed by a 31-day smoothing, as recommended by ref. ¹. The climatology periods used at SYD100 and PH100 are June 25, 2008 to April 26, 2022 (14 years) and October 27, 2009 to March 19, 2022 (13 years), respectively, determined by mooring record length at the sites.

We use in situ tide gauge (sea level) measurements provided by the Bureau of Meteorology from the Port Kembla station (BoM = 068253) located ~70 km south of Sydney at 34.47°S, 150.91°E. These quality controlled data have a resolution of 1 min and have been quality controlled and averaged as the daily mean here.

Mixed layer depths are estimated at PH100 and SYD100 using observational data products⁵² from a combination of CTD, mooring, and satellite temperature measurements. We linearly interpolate temperatures over depth to form temperature 'profiles' that are then used to estimate mixed layer depths. The temperature threshold method⁵³ is used, whereby the

mixed layer depth is defined as the depth at which the temperature of the profile is equal to the temperature at 10 m plus or minus 0.2°C .

Atmosphere and ocean reanalysis. We use the air-sea heat flux, including the net shortwave radiation, net longwave radiation, latent and sensible heat fluxes, from the European Centre for Medium-Range Weather Forecasts (ECMWF) ERA5 atmospheric reanalysis⁵⁴, with a horizontal resolution of $0.25^\circ \times 0.25^\circ$ from January 1, 1993 to 31 December, 2022. To be consistent with OSTIA, the daily and monthly climatology are computed for 1993–2022.

The three-dimensional ocean state estimates were obtained from the latest version of the daily BlueLink ReANalysis product (BRAN2020)⁵⁵. The BRAN2020 dataset has a horizontal resolution of $0.1^\circ \times 0.1^\circ$ and 51 vertical layers, realistically representing the variability of the EAC and its associated mesoscale eddies^{16,28}. We use daily velocity, temperature and mixed layer depth (h) over which the buoyancy exceeds a threshold of $0.0003 \text{ m s}^{-255}$ (computed online) from 1 January 1998 to 31 December 2022, with the climatology computed from the period of 1998–2022.

Mixed layer heat budget. The mixed layer heat budget analysis has been used successfully in the EAC region⁵⁶. To quantify the contribution of the atmosphere and ocean to the evolution of MHWs, we calculate the daily mixed layer heat budget as follows^{57,58}:

$$\underbrace{\frac{\partial T}{\partial t}}_{TTEND} = \underbrace{\frac{Q_{net} - Q_{pen}}{\rho C_p h}}_Q - \underbrace{u \frac{\partial T}{\partial x}}_{UADV} - \underbrace{v \frac{\partial T}{\partial y}}_{VADV} - \underbrace{(w_h + \frac{dh}{dt}) \frac{T - T_h}{h}}_{ENTR} + Residual \quad (1)$$

where h is the time-varying mixed layer depth, ρC_p is the volumetric heat capacity of seawater with a value of $4.088 \times 10^6 \text{ J}^\circ\text{C}^{-1}\text{m}^{-3}$. T , u and v are the vertically averaged temperature, zonal, and meridional velocity within the mixed layer. w_h and T_h are the vertical velocity and temperature at the base of the mixed layer. Q_{net} is the net heat flux at the ocean surface. The radiative heat flux penetrating through the base of the mixed layer (Q_{pen}) is a function of h and the net shortwave radiation (Q_{short}), which is defined as⁵⁸:

$$Q_{pen} = Q_{short} \left(0.58e^{-\frac{h}{0.35}} + 0.42e^{-\frac{h}{25}} \right) \quad (2)$$

The term ($TTEND$) on the left-hand side of Eq. 1 represents the temperature tendency. On the right-hand side of Eq. 1, the terms represent the contribution from the net air-sea heat flux (Q), horizontal zonal advection ($UADV$), meridional advection ($VADV$), vertical entrainment ($ENTR$) at the bottom of the mixed layer and $Residual$, respectively. The $Residual$ term includes the processes associated with the horizontal diffusion, vertical diffusion and unresolved subgrid-scale uncertainty, which is estimated by subtracting the Q , $UADV$, $VADV$, and $ENTR$ terms from the $TTEND$.

MHW definition and categories. A MHW is defined as a prolonged discrete anomalously warm water event when temperatures exceeded the 90th percentile for at least five consecutive days based on a 30-year historical baseline period¹. If the gaps between two events are <2 days, they are considered as a single continuous event. Here we calculated the daily climatology and the 90th percentile threshold for each day of the year based on the daily OSTIA over 30 years (1993–2022). Similar to previous studies²¹, daily SST were centered on the day within an 11-day window and then smoothed using a 31-day moving window. We

use a refined scheme⁵⁹ to categorize the severity of MHWs. Multiples of the local difference between the climatological mean and the 90th percentile threshold define the MHW categories as: (I) moderate (1–2×), (II) strong (2–3×), (III) severe (3–4×) and (IV) extreme (>4).

Data availability

The SST products OSTIA can be downloaded from https://data.marine.copernicus.eu/product/SST_GLO_SST_L4_NRT_OBSERVATIONS_010_001/services. The satellite altimetry products from AVISO were produced by Ssalto/Duacs and distributed by EU CMEMS and are available at https://resources.marine.copernicus.eu/product-detail/SEALEVEL_GLO_PHY_L4_MY_008_047. Integrated Marine Observing System (IMOS) Multi-sensor L3S SST data used in Fig. 2d, g can be downloaded from <http://thredds.aodn.org.au/thredds/catalog/IMOS/SRS/SST/ghrsst/L3S-1d/ngt/catalog.html>, and the in situ mooring observations are available at <https://thredds.aodn.org.au/thredds/catalog/IMOS/ANMN/NSW/catalog.html>. Sea level data at Port Kembla were provided by the Australian Bureau of Meteorology, which are available at <http://www.bom.gov.au/australia/tides/>. Air-sea heat flux were taken from the ECMWF ERA5 reanalysis product and can be accessed at <https://doi.org/10.24381/cds.f17050d7>. BRAN2020 is made freely available by CSIRO Bluelink and is supported by the Bluelink Partnership: a collaboration between the Australian Department of Defence, Bureau of Meteorology and CSIRO, which can be downloaded from <https://research.csiro.au/bluelink/outputs/data-access/>.

Code availability

All Jupyter Notebook scripts used for producing the figures will be available on Github at publication (https://github.com/lijunde/MHWs_EAC_eddies).

Received: 6 April 2023; Accepted: 2 October 2023;

Published online: 01 November 2023

References

- Hobday, A. J. et al. A hierarchical approach to defining marine heatwaves. *Prog. Oceanogr.* **141**, 227–238 (2016).
- Laufkötter, C., Zscheischler, J. & Frölicher, T. L. High-impact marine heatwaves attributable to human-induced global warming. *Science* **369**, 1621–1625 (2020).
- Frölicher, T. L., Fischer, E. M. & Gruber, N. Marine heatwaves under global warming. *Nature* **560**, 360–364 (2018).
- Smale, D. A. et al. Marine heatwaves threaten global biodiversity and the provision of ecosystem services. *Nat. Clim. Change* **9**, 306–312 (2019).
- Guo, X. et al. Threat by marine heatwaves to adaptive large marine ecosystems in an eddy-resolving model. *Nat. Clim. Change* **12**, 179–186 (2022).
- Mills, K. E. et al. Fisheries management in a changing climate: lessons from the 2012 ocean heat wave in the northwest Atlantic. *Oceanography* **26**, 191–195 (2013).
- Caputi, N. et al. Management adaptation of invertebrate fisheries to an extreme marine heat wave event at a global warming hot spot. *Ecol. Evol.* **6**, 3583–3593 (2016).
- Smith, K. E. et al. Socioeconomic impacts of marine heatwaves: global issues and opportunities. *Science* **374**, eabj3593 (2021).
- Sherman, K. Adaptive management institutions at the regional level: the case of large marine ecosystems. *Ocean Coast Manag.* **90**, 38–49 (2014).
- Hu, L. A global assessment of coastal marine heatwaves and their relation with coastal urban thermal changes. *Geophys. Res. Lett.* **48**, e2021GL093260 (2021).
- Marin, M., Feng, M., Phillips, H. E. & Bindoff, N. L. A global, multiproduct analysis of coastal marine heatwaves: distribution, characteristics, and long-term trends. *J. Geophys. Res. Oceans* **126**, e2020JC016708 (2021).
- Cook, F. et al. Marine heatwaves in shallow coastal ecosystems are coupled with the atmosphere: insights from half a century of daily in situ temperature records. *Front. Clim.* **4**, 1012022 (2022).
- Holbrook, N. J. et al. A global assessment of marine heatwaves and their drivers. *Nat. Commun.* **10**, 2624 (2019).
- Oliver, E. C. et al. Marine heatwaves. *Annu. Rev. Mar. Sci.* **13**, 313–342 (2021).
- Wu, L. et al. Enhanced warming over the global subtropical western boundary currents. *Nat. Clim. Change* **2**, 161–166 (2012).
- Li, J., Roughan, M. & Kerry, C. Drivers of ocean warming in the western boundary currents of the Southern Hemisphere. *Nat. Clim. Change* **12**, 901–909 (2022).
- Martínez-Moreno, J. et al. Global changes in oceanic mesoscale currents over the satellite altimetry record. *Nat. Clim. Change* **11**, 397–403 (2021).
- Elzahaby, Y. & Schaeffer, A. Observational insight into the subsurface anomalies of marine heatwaves. *Front. Mar. Sci.* **6**, 745 (2019).
- Elzahaby, Y., Schaeffer, A., Roughan, M. & Delaux, S. Oceanic circulation drives the deepest and longest marine heatwaves in the east Australian current system. *Geophys. Res. Lett.* **48**, e2021GL094785 (2021).
- Zhao, Z., Holbrook, N. J. & Oliver, E. C. J. An eddy pathway to marine heatwave predictability off eastern Tasmania. *Front. Clim.* **4**, 907828 (2022).
- Oliver, E. C. et al. The unprecedented 2015/16 Tasman Sea marine heatwave. *Nat. Commun.* **8**, 16101 (2017).
- Malan, N., Roughan, M. & Kerry, C. The rate of coastal temperature rise adjacent to a warming western boundary current is nonuniform with latitude. *Geophys. Res. Lett.* **48**, e2020GL090751 (2021).
- Schaeffer, A. & Roughan, M. Subsurface intensification of marine heatwaves off southeastern Australia: the role of stratification and local winds. *Geophys. Res. Lett.* **44**, 5025–5033 (2017).
- Gillett, Z. et al. The state of weather and climate extremes 2022. *ARC Centre of Excellence for Climate Extremes, UNSW, Sydney, Australia.* (2023).
- Cetina-Heredia, P., Roughan, M., Sebille, E. V. & Coleman, M. A. Long-term trends in the East Australian Current separation latitude and eddy driven transport. *J. Geophys. Res. Oceans* **119**, 4351–4366 (2014).
- Li, J., Roughan, M. & Kerry, C. Dynamics of interannual eddy kinetic energy modulations in a western boundary current. *Geophys. Res. Lett.* **48**, e2021GL094115 (2021).
- Li, J., Roughan, M. & Kerry, C. Variability and drivers of ocean temperature extremes in a warming western boundary current. *J. Clim.* **35**, 1097–1111 (2022).
- Li, J. & Roughan, M. Energetics of eddy-mean flow interactions in the east Australian current system. *J. Phys. Oceanogr.* **53**, 595–612 (2023).
- Pilo, G. S., Mata, M. M. & Azevedo, J. L. L. Eddy surface properties and propagation at Southern Hemisphere western boundary current systems. *Ocean Sci.* **11**, 629–641 (2015).
- Cetina-Heredia, P., Roughan, M., van Sebille, E., Keating, S. & Brassington, G. B. Retention and leakage of water by mesoscale eddies in the east Australian current system. *J. Geophys. Res. Oceans* **124**, 2485–2500 (2019).
- Ribbat, N., Roughan, M., Powell, B., Rao, S. & Kerry, C. G. Transport variability over the Hawkesbury Shelf (31.5–34.5°S) driven by the East Australian Current. *PLoS ONE* **15**, e0241622 (2020).
- Roughan, M., Cetina-Heredia, P., Ribbat, N. & Suthers, I. M. Shelf transport pathways adjacent to the east Australian current reveal sources of productivity for coastal reefs. *Front. Mar. Sci.* **8**, 789687 (2022).
- Malan, N., Roughan, M., Hemming, M. & Schaeffer, A. Mesoscale circulation controls chlorophyll concentrations in the east Australian current separation zone. *J. Geophys. Res. Oceans* **128**, e2022JC019361 (2023).
- Schaeffer, A., Gramouille, A., Roughan, M. & Mantovanelli, A. Characterizing frontal eddies along the East Australian Current from HF radar observations. *J. Geophys. Res. Oceans* **122**, 3964–3980 (2017).
- Roughan, M. et al. A tale of two eddies: the biophysical characteristics of two contrasting cyclonic eddies in the East Australian Current System. *J. Geophys. Res. Oceans* **122**, 2494–2518 (2017).
- Suthers, I. M. et al. Frontal eddies provide an oceanographic triad for favourable larval fish habitat. *Limnol. Oceanogr.* **68**, 1019–1036 (2023).
- Malan, N. et al. Eddy-driven cross-shelf transport in the east Australian current separation zone. *J. Geophys. Res. Oceans* **125**, e2019JC015613 (2020).
- Archer, M. et al. Observations of submesoscale variability and frontal subduction within the mesoscale eddy field of the Tasman Sea. *J. Phys. Oceanogr.* **50**, 1509–1529 (2020).
- Roughan, M. & Middleton, J. H. On the East Australian Current: variability, encroachment, and upwelling. *J. Geophys. Res. Oceans* **109**, C07003 (2004).
- Archer, M. R., Roughan, M., Keating, S. R. & Schaeffer, A. On the variability of the east Australian current: jet structure, meandering, and influence on shelf circulation. *J. Geophys. Res. Oceans* **122**, 8464–8481 (2017).
- Oke, P. R. & Griffin, D. A. The cold-core eddy and strong upwelling off the coast of New South Wales in early 2007. *Deep-Sea Res. Part II Top. Stud. Oceanogr.* **58**, 574–591 (2011).
- Schaeffer, A., Roughan, M. & Morris, B. D. Cross-shelf dynamics in a western boundary current regime: Implications for upwelling. *J. Phys. Oceanogr.* **43**, 1042–1059 (2013).
- Li, J., Roughan, M., Kerry, C. & Rao, S. Impact of mesoscale circulation on the structure of river plumes during large rainfall events inshore of the east Australian current. *Front. Mar. Sci.* **9**, 815348 (2022).
- Malan, N., Roughan, M., Stanley, G. J., Holmes, R. & Li, J. Quantifying cross-shelf transport in the East Australian Current System: a budget-based approach. *J. Phys. Oceanogr.* **52**, 2555–2572 (2022).
- Wei, X., Li, K.-Y., Kilpatrick, T., Wang, M. & Xie, S.-P. Large-scale conditions for the record-setting southern California marine heatwave of August 2018. *Geophys. Res. Lett.* **48**, e2020GL091803 (2021).

46. Cooley, K. M., Fewings, M. R., Lerczak, J. A., O'Neill, L. W. & Brown, K. S. Role of sea surface physical processes in mixed-layer temperature changes during summer marine heat waves in the Chile-Peru current system. *J. Geophys. Res. Oceans* **127**, e2021JC018338 (2022).
47. Manta, G., de Mello, S., Trinchin, R., Badagian, J. & Barreiro, M. The 2017 record marine heatwave in the southwestern Atlantic shelf. *Geophys. Res. Lett.* **45**, 449–456 (2018).
48. Good, S. et al. The current configuration of the ostia system for operational production of foundation sea surface temperature and ice concentration analyses. *Remote Sens.* **12**, 720 (2020).
49. Ducet, N., Le Traon, P. Y. & Reverdin, G. Global high-resolution mapping of ocean circulation from TOPEX/Poseidon and ERS-1 and -2. *J. Geophys. Res. Oceans* **105**, 19477–19498 (2000).
50. Oliver, E. C., O'Kane, T. J. & Holbrook, N. J. Projected changes to Tasman Sea eddies in a future climate. *J. Geophys. Res. Oceans* **120**, 7150–7165 (2015).
51. Roughan, M., Schaeffer, A. & Suthers, I. M. Chapter 6 - Sustained Ocean Observing along the Coast of Southeastern Australia: NSW-IMOS 2007-2014. In Liu, Y., Kerkering, H. & Weisberg, R. H. (eds.) *Coastal Ocean Observing Systems*, 76–98 (Academic Press, 2015).
52. Roughan, M. et al. Multi-decadal ocean temperature time-series and climatologies from Australia's long-term national reference stations. *Sci. Data* **9**, 157 (2022).
53. de Boyer Montégut, C., Madec, G., Fischer, A. S., Lazar, A. & Iudicone, D. Mixed layer depth over the global ocean: an examination of profile data and a profile-based climatology. *J. Geophys. Res.: Oceans* **109** (2004).
54. Hersbach, H. et al. The ERA5 global reanalysis. *Q. J. R. Meteorol. Soc.* **146**, 1999–2049 (2020).
55. Chamberlain, M. A. et al. Next generation of Bluelink ocean reanalysis with multiscale data assimilation: BRAN2020. *Earth Syst. Sci. Data* **13**, 5663–5688 (2021).
56. Elzahaby, Y., Schaeffer, A., Roughan, M. & Delaux, S. Why the mixed layer depth matters when diagnosing marine heatwave drivers using a heat budget approach. *Front. Clim.* **4**, 838017 (2022).
57. Cronin, M. F., Pelland, N. A., Emerson, S. R. & Crawford, W. R. Estimating diffusivity from the mixed layer heat and salt balances in the North Pacific. *J. Geophys. Res. Oceans* **120**, 7346–7362 (2015).
58. Shi, J. et al. Role of mixed layer depth in the location and development of the northeast Pacific warm blobs. *Geophys. Res. Lett.* **49**, e2022GL098849 (2022).
59. Hobday, A. J. et al. Categorizing and naming marine heatwaves. *Oceanography* **31**, 162–173 (2018).

Acknowledgements

We are grateful for the ongoing contributions of the NSW IMOS moorings team, who maintain the PH100 and SYD100 moorings. This research is partially supported by an Australian Research Council Discovery Project (DP230100505), the Australian Research Council, Centre of Excellence for Climate Extremes (CE170100023) and the Fundamental Research Funds for the Central Universities, China (1074-423102). Data were

sourced from Australia's Integrated Marine Observing System (IMOS)-IMOS is enabled by the National Collaborative Research Infrastructure Strategy (NCRIS). This research was undertaken with the assistance of resources and services from the National Computational Infrastructure (NCI), which is supported by the Australian Government. This research also includes computations using the computational cluster Katana (<https://doi.org/10.26190/669x-a286>) supported by Research Technology Services at UNSW Sydney.

Author contributions

J.L. and M.R. conceived the study and developed the conceptual framework. J.L. conducted the analysis and wrote the first draft. M.H. created Fig. 2. All authors contributed to interpreting the results, writing and editing the manuscript.

Competing interests

The authors declare no competing interests.

Additional information

Supplementary information The online version contains supplementary material available at <https://doi.org/10.1038/s43247-023-01041-8>.

Correspondence and requests for materials should be addressed to Junde Li.

Peer review information *Communications Earth & Environment* thanks Marlos Goes, Gaston Manta and the other, anonymous, reviewer(s) for their contribution to the peer review of this work. Primary Handling Editors: Regina Rodrigues, Heike Langenberg. A peer review file is available.

Reprints and permission information is available at <http://www.nature.com/reprints>

Publisher's note Springer Nature remains neutral with regard to jurisdictional claims in published maps and institutional affiliations.



Open Access This article is licensed under a Creative Commons Attribution 4.0 International License, which permits use, sharing, adaptation, distribution and reproduction in any medium or format, as long as you give appropriate credit to the original author(s) and the source, provide a link to the Creative Commons license, and indicate if changes were made. The images or other third party material in this article are included in the article's Creative Commons license, unless indicated otherwise in a credit line to the material. If material is not included in the article's Creative Commons license and your intended use is not permitted by statutory regulation or exceeds the permitted use, you will need to obtain permission directly from the copyright holder. To view a copy of this license, visit <http://creativecommons.org/licenses/by/4.0/>.

© The Author(s) 2023